Articles

Disorder-to-Order Transition of the Active Site of Human Class Pi Glutathione Transferase, GST P1-1†

T. Kevin Hitchens,‡ Bengt Mannervik,§ and Gordon S. Rule*,‡

Department of Biological Sciences, Carnegie Mellon University, 4400 Fifth Avenue, Pittsburgh, Pennsylvania 15213, and Department of Biochemistry, Uppsala University, Biomedical Center, Box 576, SE-751 23, Uppsala, Sweden

Received May 3, 2001; Revised Manuscript Received July 17, 2001

ABSTRACT: Glutathione transferases comprise a large family of cellular detoxification enzymes that function by catalyzing the conjugation of glutathione (GSH) to electron-deficient centers on carcinogens and other toxins. NMR methods have been used to characterize the structure and dynamics of a human class pi enzyme, GST P1-1, in solution. Resonance assignments have been obtained for the unliganded enzyme and the GSH and *S*-hexylglutathione (GS-hexyl) complexes. Differences in chemical shifts between the GSH and GS-hexyl complexes suggest more extensive structural differences between these two enzyme−ligand complexes than detected by previous crystallographic methods. The NMR studies reported here clearly show that an α-helix (α2) within the GSH binding site exists in multiple conformations at physiological temperatures in the absence of ligand. A single conformation of α2 is induced by the presence of either GSH or GS-hexyl or a reduction in temperature to below 290 K. The large enthalpy of the transition (∼150 kJ/mol) suggests a considerable structural rearrangement of the protein. The Gibbs free energy for the transition to the unfolded form is on the order of −4 to −6 kJ/mol at physiological temperatures (37 °C). This order-to-disorder transition contributes substantially to the overall thermodynamics of ligand binding and should be considered in the design of selective inhibitors of class pi glutathione transferases.

Glutathione transferases (GSTs)[1] are a family of cellular detoxification enzymes that catalyze the conjugation of glutathione (GSH, L-γ-glutamylcysteinylglycine) to a wide range of hydrophobic compounds, including carcinogens and other toxins (see refs *1*−*3* for review). These enzymes have been grouped into distinct classes on the basis of sequence and structural homology, immunochemistry, and substrate specificity. There are at least eight classes of cytosolic mammalian GSTs: alpha, mu, pi, sigma, theta, kappa, omega, and zeta (*4*−*9*). The existence of numerous isoenzymes is largely responsible for the broad substrate specificity of GSTs. Remarkably, additional breadth in specificity is attained by the catalytic competency of any single GST toward a number of chemically unique substrates.

Crystal structures of numerous GSTs have provided a wealth of structural information on unliganded and liganded forms of these enzymes (*9*−*20*, see ref *21* for review). All cytosolic GSTs are dimeric enzymes containing one active site per monomer. The individual monomers may be further divided into two domains. The N-terminal domain contains 70−90 residues in an α-β motif with the following order of secondary structural elements: β1-α1-β2-α2-β3-β4-α3. The N-terminal domain interacts more extensively with the bound GSH. Mutagenesis studies of the human class pi enzyme have identified a number of residues in this domain that are important for the binding of GSH (*22*). These include Arg14,[2] Lys45, Gln52, Gln65, and Asp99. The C-terminal domain consists of approximately 120 residues and is largely α-helical. This domain is largely responsible for the binding of hydrophobic substrates. Several amino acid residues in the hydrophobic binding site have been implicated in substrate binding and/or catalysis. For example, in the human class pi enzyme, alteration of Tyr109 to Phe affects the catalytic activity of the enzyme toward some substrates, but not others (*23*).

Although all soluble GSTs share a common architecture, there are topological features of the active site that are unique

† This work was supported by the Eberly Family Professorship in Structural Biology to G.S.R., a National Institutes of Health NSRA fellowship to T.K.H., and the Swedish Natural Science Research Council (B.M.). The 600 MHz spectrometer was obtained through an equipment grant from the NIH (S100 RR11248-01).

* To whom correspondence should be addressed. E-mail: rule@andrew.cmu.edu, Phone: 412-268-1839.

‡ Carnegie Mellon University.

§ Uppsala University.

[1] Abbreviations: GSH, glutathione (L-γ-glutamylcysteinylglycine); GS-hexyl, *S*-1-hexylglutathione; GST, glutathione transferase; GST P1-1, homodimeric human class pi GST P1; HMQC, heteronuclear multiple-quantum coherence; IPTG, isopropyl-β-D-thiogalactopyranoside; NMR, nuclear magnetic resonance.

[2] The residue numbering scheme includes the amino-terminal Met residue as the first residue.

10.1021/bi010909+ CCC: $20.00 © 2001 American Chemical Society
Published on Web 09/06/2001

to specific classes. One of the major topological differences between isoenzyme classes occurs in the segment that links β2 to α2. In the class mu enzymes, this segment forms an extended solvent-exposed loop (mu-loop) that partially occludes the active site. The corresponding segment in the class pi enzyme is a short α-helix that is customarily considered to be part of α2. The second major site of topological variability occurs at the carboxy terminus. Class pi enzymes possess a relatively small carboxy terminus, the carboxy terminus of class mu enzymes forms an Ω-loop that partially occludes the active site, and the carboxy termini of class alpha and theta enzymes exist as well-defined α-helices that severely occlude the active site. The existence of structural features that occlude the active site indicates that protein dynamics may play an important role in the catalytic cycle of many of these enzymes. The diverse topology of this group of enzymes provides a unique opportunity to explore the importance of structural dynamics in enzyme catalysis within the context of a common underlying structural framework.

We have previously investigated the dynamic properties of a human class mu enzyme, GST M2-2, using solution NMR methods. These studies showed that the mu-loop of this enzyme is well structured in both the presence and the absence of ligand and undergoes fluctuations in orientation on the microsecond to nanosecond time scale (*24*). These fluctuations may be important for substrate binding and product release. In addition, it was shown in those studies that extensive motion of the carboxy-terminal Ω-loop does not occur (*24*).

Extensive ligand induced disorder-to-order transitions may exist in several classes of glutathione transferases. In the rat theta enzyme, GST T2-2, kinetic studies give evidence for conformational changes of the protein during the catalytic mechanism (*25*). X-ray diffraction studies of a human class alpha enzyme (A1-1) suggest that its carboxy-terminal helix is disordered in unliganded enzyme, but becomes ordered in the presence of ligand (*11, 12*). Several lines of evidence suggest that the second alpha helix (α2) in the human class pi enzyme GST P1-1 behaves in a similar manner. The X-ray crystal structure of GST P1-1 lacks discernible electron density for α2 in the absence of ligand (*17*). Time-resolved fluorescence studies of a Trp residue within α2 (Trp39) suggest the presence of two predominant conformational states in the absence of glutathione. One of these states reflects a solvent-exposed environment of the tryptophan side chain while the second state suggests that the tryptophan side chain is in an apolar environment (*27*). Additional evidence for the conformational fluctuations of α2 has also been provided by chemical reactivity and fluorescence energy transfer experiments. The chemical reactivity of a cysteine residue in α2 (Cys48) is dependent on viscosity, suggesting a coupling between diffusive movements of the enzyme and the reactivity of the thiol group (*28*). The formation of a disulfide bond between Cys48 and Cys102, which are 18 Å apart in the enzyme−ligand complex, occurs in the absence of ligand (*29*). Fluorescence energy transfer experiments indicate that the distance between Cys101 and residues Trp29 and Trp39 increases upon GSH binding (*28*). Molecular dynamics calculations also support considerable flexibility within α2 (*30, 31*). Although these studies provide evidence for glutathione-induced changes in the environment of Trp39 and Cys48, they are naturally limited to a small number of sites in α2 and cannot report on conformational changes that occur on time scales much slower than nanoseconds.

The binding of GSH may be coupled to the different conformational states of α2 in the class pi enzyme. Lo Bello et al. (*32*) altered both Gly42 and Gly51 to Ala and observed a 100-fold reduction in the affinity of GSH as well as the establishment of positive cooperativity in binding. These changes in GSH affinity were ascribed to structural changes that lead to a more occluded active site. Temperature effects on GSH binding and cooperativity have also been noted (*33*), indicative of temperature-induced conformational changes in the GSH binding site, possibly involving α2.

The existence of disordered helices in the unliganded alpha and pi class enzymes is a specific example of the general phenomenon of disorder−order transitions that are known to exist in other proteins (*34*). In this particular case, the enzyme can utilize the significant decrease in the entropy that occurs upon GSH binding to facilitate product release. Consequently, it is important to characterize the structural and thermodynamic aspects of this transition as an important component of the overall catalytic mechanism of these enzymes. The human class pi enzyme, GST P1-1, is of particular interest for drug design (*35*), since it has been implicated in the development of cellular multi-drug resistance to a number of chemotherapeutic agents (*36*−*41*).

To date, the most substantial evidence for disorder−order transitions in class alpha and pi enzymes has been from X-ray crystallographic studies. However, as with all crystallographic studies, it is not possible to distinguish whether static disorder or motion is responsible for the lack of electron density. In contrast, NMR techniques are broadly applicable to the characterization of dynamic processes in proteins over a large range of time scales. In this paper, we apply NMR methods to probe the putative disorder-to-order transition of α2 of the human pi class GST P1-1. We have used a combination of protein deuteration, triple resonance NMR techniques, and site-specific labeling to assign the amide resonances of the 46 kDa GST P1-1 in the unliganded form of the protein, the GSH complex, and the complex with a competitive inhibitor, *S*-hexylglutathione (GS-hexyl).[3] These experiments indicate that α2 is disordered in the unliganded enzyme at temperatures above 20 °C, but assumes a well-defined structure at lower temperatures or in the presence of GSH or *S*-hexylglutathione. The relatively large enthalpy of this disorder-to-order transition suggests a significant structural rearrangement of the enzyme when ligand binds.

MATERIALS AND METHODS

Sample Preparation. High-level expression of human GST P1-1 in *E. coli* (JM109) was obtained from the expression vector pKXHP1 (*42*). This vector routinely yielded 50−100 mg of purified enzyme per liter of culture. Production of GST P1-1 was induced by the addition of 1.0 mM IPTG (isopropyl β-D-thiogalactopyranoside) when the cells reached an $OD_{\lambda=550}$ between 0.5 and 1.0. After 12−18 h of induction, the cells were harvested and lysed by sonication, and the

[3] Chemical shifts are available by request from the corresponding author.

lysate was clarified by centrifugation (20 000 rpm, Beckman Ti70 rotor, 20 min). The lysate was then chromatographed at 5 °C on a DEAE Sephadex (Pharmacia) column using a linear 0−0.5 M NaCl gradient in a buffer that contained 25 mM Tris (pH 7.5, all pH values at 20 °C) and 10 mM β-mercaptoethanol. The pooled fractions were loaded onto a GS-hexyl affinity column (Sigma) that was equilibrated with 25 mM Tris (pH 7.5), 2 mM EDTA, and 10 mM β-mercaptoethanol. The bound enzyme was eluted with 50 mM Tris (pH 8.0), 5 mM GSH, and 10 mM β-mercaptoethanol. Enzyme fractions were checked for activity toward 1-chloro-2,4-dinitrobenzene according to Habig and Jakoby (*43*). The active fractions were concentrated and exchanged into NMR buffer (10 mM phosphate, 25 μM EDTA, 100 μM dithioerythritol, 50 mM NaCl, pH 7.0) using ultrafiltration devices (Amicon). When appropriate, the NMR buffer contained either 10 mM GSH or 5 mM GS-hexyl.

Isotopically labeled samples of GST P1-1 were prepared in a manner similar to the methods that were previously described for the GST M2-2 (*26*). All isotopes were purchased from Cambridge Isotopes Laboratories, Inc. (CIL, Andover, MA). GST P1-1, deuterated to approximately 85%, was used for all experiments except where noted. This level of deuteration was achieved by growing the *E. coli* host in minimal media containing 4 g/L glucose, 1 g/L ammonium sulfate, and 98% ^2H_2O (see ref *26* for details). Perdeuterated ^{13}C-^{15}N-labeled protein was prepared by expression in minimal media containing [^2H-^{13}C]glucose as the sole carbon source. Previously, we had used Bio-Express cell growth media (CIL) to produce a class mu GST (GST M2-2) using a temperature-sensitive expression system (*26*). However, in the case of this particular expression vector for GST P1-1, we found that the Bio-Express media induced high levels of the protein in the absence of the normal inducer (IPTG), leading to premature cell death.

Samples uniformly labeled with ^{15}N and specifically labeled at the carbonyl carbon (1-^{13}C) of Tyr, Phe, Ala, Ile, Lys, or Val were prepared as described previously (*26*). Samples labeled with [1-^{13}C]-Pro were obtained by adding 100 mg/L of the labeled compound 30 min before induction. In the case of Ser and Gly, the scrambling of isotopic label was reduced by using growth media containing 100 mg/L Ser (labeled or unlabeled), 100 mg/L Gly (unlabeled or labeled), 100 mg/L unlabeled Cys, and 10 μM adenosine and guanosine.

NMR Spectroscopy. NMR spectra were recorded at 600 MHz (^1H) using a Bruker DRX spectrometer equipped with deuterium decoupling and Bruker triple-resonance probes with triple axis pulsed-field gradient coils. Unless otherwise noted, all spectra were recorded at 306 K. Homonuclear NOE mixing times were 100−150 ms. Quadrature detection was obtained using the States-TPPI method (*44*). The recycle delay for most NMR experiments was 1.3 s. Pulsed field gradients were used to suppress undesired coherences and water magnetization (*45*). Water suppression schemes generally included gradients applied as ZZ-filters and a "watergate" selection for off-resonance signals (*46*). The following triple-resonance experiments were used for resonance assignment purposes: HNCA, HN(CO)CA, HN(CA)CB, HNCO, and HN(CA)CO. Typical sweepwidths for the indirectly detected domains were 26 ppm for ^{15}N (32 complex points) and 30 ppm for ^{13}C (64 complex points). The number of scans varied from 16 [HNCA, HN(CO)CA] to 32 [HN(CA)CO, HN(CA)CB], depending on the experiment. The 4-dimensional ^1H-^{15}N-^{15}N-^1H-separated NOESY experiment was acquired with 20 complex points in each ^{15}N dimension and with 64 complex points in the indirectly detected ^1H dimension. Two scans were acquired per time point, giving an overall experiment time of approximately 4 days. A higher resolution 3-dimensional version of the 4D NOESY was acquired with 64 complex points in the indirectly detected ^{15}N dimension. Additional details regarding the above experiments as well as primary literature references can be found in McCallum et al. (*26*). A pulse sequence that results in the minimal suppression of the water magnetization was utilized for HMQC spectra (*47*). NMR spectra were processed and analyzed as described previously (*26*) using FELIX 97.0 (Molecular Simulations Inc., San Diego, CA) software on a R4400 Silicon Graphics workstation.

Chemical Shift Assignments. Chemical shift assignments were first obtained for the GS-hexyl complex. Inter- and intraresidue C_α chemical shifts were obtained from HNCA and HN(CO)CA experiments. Inter- and intraresidue C_β chemical shifts were obtained from a NH(CA)CB experiment. CO chemical shifts were obtained from HNCO (interresidue) and HN(CA)CO (intraresidue) experiments. These chemical shifts were used as constraints in our in-house Monte Carlo assignment program (see refs *24*, *26*). This program utilizes interresidue chemical shift connectivities derived from *J*-coupled experiments (e.g., HNCA), through-space connectivities from NOESY experiments, residue type prediction based on chemical shift and secondary structure, and information from specifically labeled samples to obtain resonance assignments. We utilized the known crystal structure of the GST P1-1 enzyme (*18*, 1AQW) to guide the use of connectivity information from the NOESY experiment. A 1-^{13}C specific labeling scheme and a 2D ^1H-^{15}N HNCO experiment were used to identify 8 of the 12 Tyr, 8 of the 15 Ala, 3 of the 7 Phe, 13 of the 32 Leu, 7 of the 14 Val, 3 of the 7 Ile, 7 of the 12 Lys, 5 of the 10 Pro, 11 of the 18 Gly, and 5 of the 10 Ser residues in the protein (*26*). The missing residues from the 2D HNCO experiments on 1-^{13}C-labeled samples are a result of slow ^2H-to-^1H amide exchange following expression in deuterated media.

The assignments for the unliganded protein at 306 K were obtained using the same information that was used for the assignment of the GS-hexyl complex. In addition, the chemical shifts from the GS-hexyl complex were utilized to guide the assignments during the Monte Carlo protocol. The assumption here is that the added ligand results in only a small perturbation of the chemical shift of residues that are distant to the binding site. This chemical shift matching was added to the Monte Carlo protocol by comparing the locations of cross-peaks in the three-dimensional HNCA, HNCO, and HN(CA)CB spectra of liganded and unliganded samples. For example, if the N_H, H_N, and C_α chemical shifts of a trial assignment for a spin-system in the unliganded sample matched the known assignments from the GS-hexyl complex, then the trial assignment was scored favorably by the Monte Carlo program. However, if a single chemical shift, either proton, nitrogen, or carbon, was greater than the allowed tolerance, the two cross-peaks were not considered to match and did not contribute to the solution. Resonance

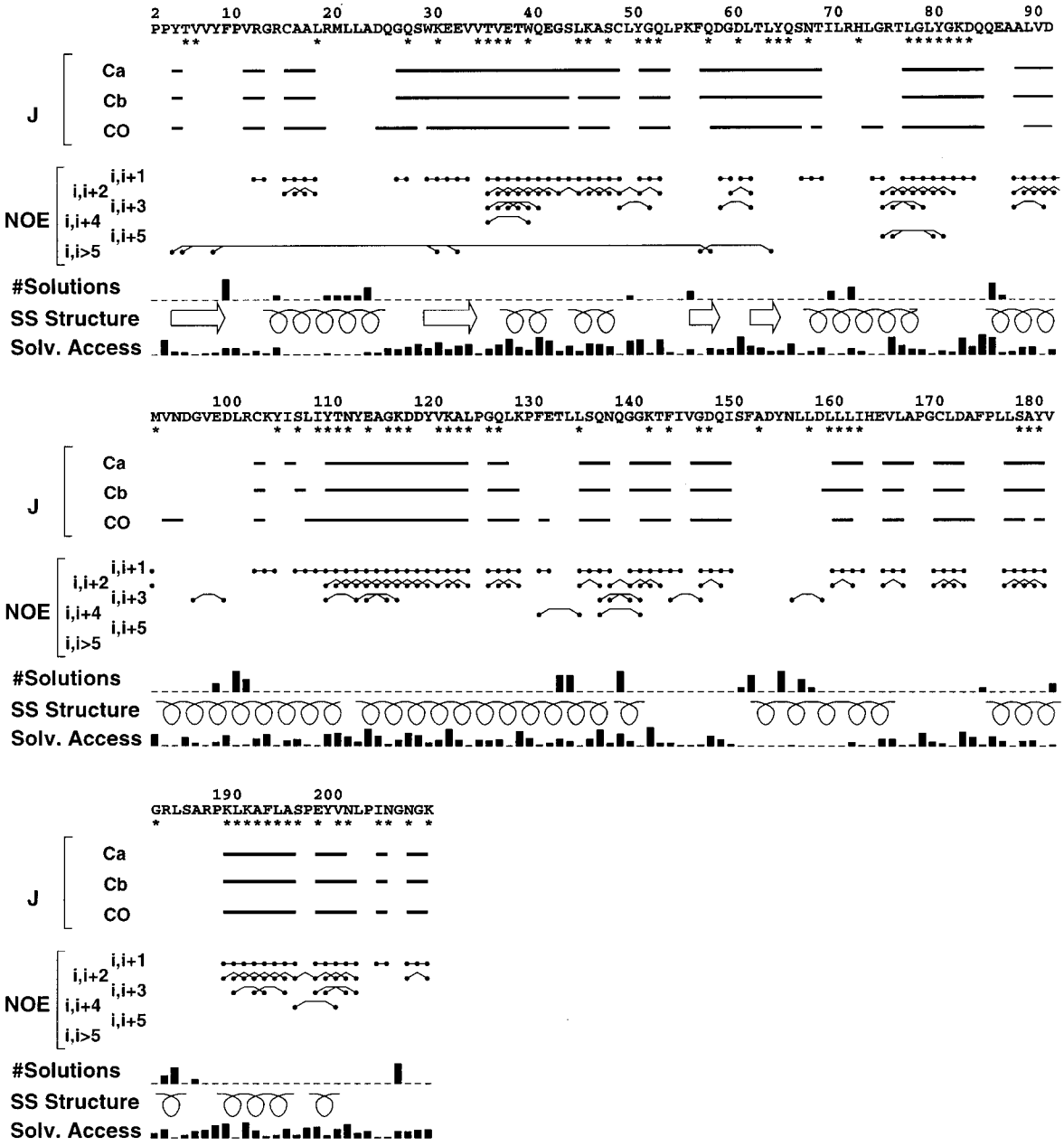

FIGURE 1: Summary of information used to assign GST P1-1 in complex with GS-hexyl. The top line shows the primary structure of the protein. An asterisk below a residue indicates that the residue type for this spin-system was obtained from specific 1-^{13}C labeling. The interresidue C_α, C_β, and CO connectivities are shown as horizontal bars. These were identified using HNCA, HNCOCA, HNCB, HNCO, and HNCACO experiments, respectively. Observed NOE connectivities between amide groups are categorized and displayed as (i+1), (i+2), (i+3), (i+4), (i+5), and long range (i>5). The number of occurrences of alternative assignments for a particular residue are displayed as a vertical bar (#Solutions); a zero height bar is indicative of an unambiguous and unique assignment. A nonzero height bar represents ambiguity in the assignment for this residue; a number of different amide resonances gave acceptable scores in the Monte Carlo program. The solvent-exposed surface area of a residue (Solv. Access) is represented as vertical bars; a higher bar indicates greater solvent exposure. The solvent accessibility was calculated from the crystal structure of the dimer using the surface program MS with a 1.4 Å probe (*58*). The secondary structure of the protein is also shown (SS Structure). The coils represent α-helices, and the arrows represent β-strands.

assignments for residues of helix α2 in the unliganded protein at 288 K were obtained by comparing N, H_N, C_α, and CO chemical shifts to the chemical shifts obtained for the GS-hexyl complex at 306 K. In addition, C_α connectivity information was used to further verify these resonance assignments.

The assignment of the GSH complex was accomplished using only interresidue C_α connectivities and by a comparison of HNCA and HNCO chemical shifts between the GSH complex and the GS-hexyl complex, as described above.

RESULTS

Resonance Assignments. The majority of the solvent-accessible amide resonance peaks for GST P1-1 in complex with GS-hexyl or GSH have been reliably assigned. The connectivity information used for the assignment of the GS-hexyl complex is summarized in Figure 1. Several regions of the protein near the active site are unambiguously assigned, including α2 (residues 36−52), the carboxy-terminal end of the fourth helix (residues 107−111), and

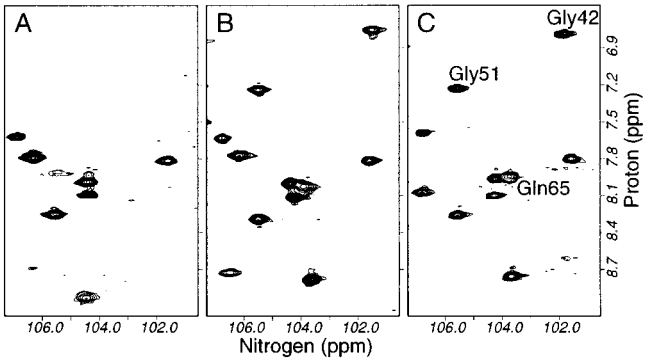

FIGURE 2: Ligand binding causes the appearance of NMR signals from α2. Sections of the two-dimensional ^{1}H-^{15}N HMQC spectra of GST P1-1 are shown for samples without ligand (panel A) and in the presence of saturating levels of GSH (panel B) or GS-hexyl (panel C). All spectra were acquired at 306 K on 1.0−1.5 mM samples of GST P1-1 (monomer concentration). Resonance lines that appear in the ligand-bound enzyme are labeled in panel C with the residue number of the corresponding amino acid. These resonances are also seen in the GSH sample (panel B) at similar chemical shifts, but are absent in panel A.

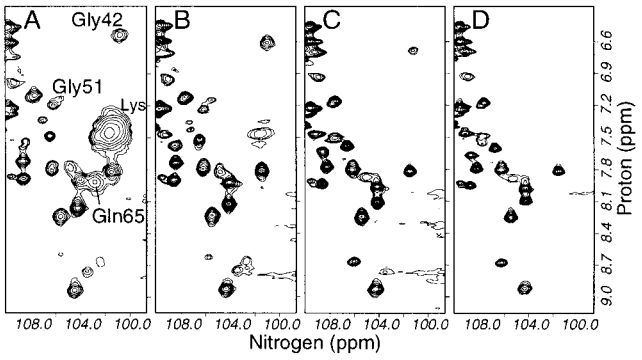

FIGURE 3: Effect of temperature on the appearance of NMR signals from α2. Sections of the two-dimensional ^{1}H-^{15}N HMQC spectra of GST P1-1 are shown for samples without ligand at various temperatures: 278 K (panel A), 288 K (panel B), 298 K (panel C), 303 K (panel D). Resonance peaks of residues Gly42, Gly51, and Gln65 are present in spectra acquired at low temperatures, but disappear at high temperatures. The large resonance peak that is observed in the spectra acquired at 278 K, labeled Lys, arises from the side chain amino groups of lysine that have been aliased twice.

the carboxy terminus. Residues in the floor of the active site (residues 8−14) are not reliably assigned by the data. The H_N, N, C_α, and CO chemical shifts obtained for the GSH complex correlated well with the assignments determined for the GS-hexyl complex. In this case, only C_α connectivity information was used to confirm the assignments. Of particular interest here is that the residues contained within α2 were assigned with a high degree of confidence in both the GSH and GS-hexyl complexes.

In the case of the unliganded enzyme at 306 K, the chemical shift assignments for residues in the top of the fourth helix and in the carboxy terminus are found to be as reliable as those obtained for the GSH and GS-hexyl complexes (data not shown). However, in unliganded GST P1-1 at 306 K, it was not possible to identify the amide resonance peaks for a large number of residues in α2. Figure 2 shows a section of the HMQC spectrum, acquired at 306 K, from unliganded enzyme, the GSH complex, and the GS-hexyl complex. The labeled peaks, Gly42, Gly51, and Gln65, are observable when either GSH or GS-hexyl are present, but cannot be observed in the absence of ligand at this temperature. We also observe similar behavior for Val34 as well as the indole NH of Trp39. All of these residues either are contained in or are in close proximity to helix α2.

Effect of Temperature on the HMQC Spectrum of Unliganded GST P1-1. The absence of resonance assignments for residues in α2 in the unliganded GST P1-1 prompted a detailed study of the effect of temperature on the HMQC spectrum of unliganded enzyme and the GS-hexyl complex. The HMQC spectrum of the GS-hexyl complex is largely unchanged as a function of temperature. The only differences observed in the spectra acquired between 278 and 306 K are some small chemical shift changes and increased resonance line widths at lower temperatures due to increased solution viscosity (data not shown). In contrast, the HMQC spectra of the unliganded GST P1-1 show extensive and reversible changes over this temperature range. Figure 3 shows a region of the HMQC spectrum for data acquired at four different temperatures. Resonance peaks from Gly42, Gly51, and Gln65 are present in spectra acquired at low temperatures, but disappear at higher temperatures. Resonances from Val34 and the indole of Trp39 also exhibit the same behavior (data not shown). All of these resonance peaks become clearly observable when either GSH or GS-hexyl is bound, regardless of the temperature of the sample.

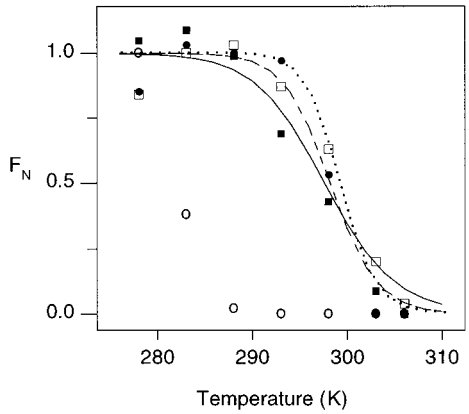

FIGURE 4: Temperature dependence of the intensity of resonance lines suggests a highly cooperative transition. The normalized intensities of the NH resonance signals from Gly42 (●), Val34 (■), Trp39 indole (□), and Gln65 (○) are shown as a function of temperature. The solid, dashed, and dotted lines represent transition curves that would be obtained for ΔH° values of +150, +200, and +250 kJ/mol, respectively. The corresponding entropy values are 505, 672, and 840 J/(mol·deg), respectively.

If a simple two-state transition is assumed for the change in enzyme structure at low versus high temperatures, then it is possible to extract thermodynamic parameters from the temperature dependence of the resonance line intensity. The fraction of the protein in the folded conformational state, F_N, can be obtained from the intensity of resonance lines that are visible at low temperatures, but disappear at higher temperatures. In the HMQC spectrum of GST P1-1, there are several well-resolved resonance peaks than may be used to report on the transition. Figure 4 shows the temperature dependence for the intensities of the amide resonance peaks for Gly42, Val34, and Gln65 and the indole resonance peak of Trp39. It was difficult to quantify the intensity of Gly51 because of resonance overlap; however, the behavior of this residue is qualitatively similar to that of Gly42, Val34, and Trp39.

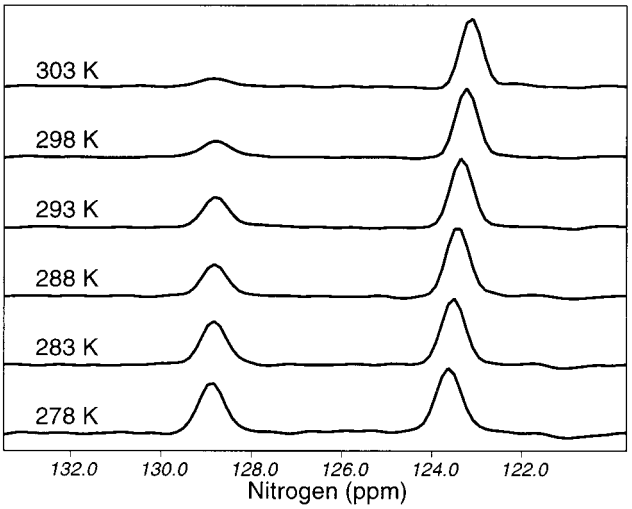

FIGURE 5: Temperature has a small effect on the width of the resonance line from Trp38. Resonance lines from the indole NH of Trp39 (left line) and the NH of Leu176 (right line) are shown for temperatures ranging from 278 K (bottom spectrum) to 303 K (top spectrum). The width of the resonance from Leu176 is 34 Hz at 278 K and narrows to 28 Hz at 303 K. The width of resonance from the indole of Trp39 is also 34 Hz at 278 K, but broadens to 40 Hz at 303 K.

The three lines in Figure 4 represent three possible fits of a two-state transition to the data obtained for Gly42, Val34, and Trp39. All three solutions exhibit approximately the same χ^2 values, ranging from 1 to 2.0 (assuming a 10% error in peak intensity) and represent $\Delta H°$ values for unfolding of +150, +200, or +250 kJ/mol for the solid, dashed, and dotted lines, respectively. It is not possible to define the $\Delta H°$ for this transition with higher accuracy due to the sensitivity of the fitted parameters to the shape of the curve. In addition, a slight amount of protein aggregation at higher temperatures makes the transition appear slightly sharper, resulting in artificially higher $\Delta H°$ values. For purposes of discussion, we will use the lower value of +150 kJ/mol. This large value of $\Delta H°$ suggests that the observed temperature-induced changes in the NMR spectrum of GST P1-1 are not simply due to changes in the amide exchange rate of exposed residues in α2. This conclusion is also supported by line width measurements presented below.

There is little change in the line width for these resonance peaks as a function of temperature, suggesting that the conformational state observed at low temperatures is in slow exchange with the conformational state(s) present at higher temperatures. Figure 5 shows the temperature dependence of the line shape for resonances from the indole of Trp39 and for Leu176 (a residue distant from the binding site). The resonance from Trp39 shows a small degree of line-broadening at 303 K, likely reflecting motion of the side chain. In the case of Gly42, the ^{15}N line width decreases from 49 Hz at 278 K to 40 Hz at 298 K (data not shown). This decrease in line width as the temperature is raised can be fully accounted for by the decrease in the rotational correlation time of the enzyme.

The thermodynamics of this transition as detected by Gln65 are considerably different than the residues in α2. The amide resonance line for this residue is broad and may be affected by additional factors beyond the disorder−order transition sensed by the other four residues within α2.

DISCUSSION

Large proteins, such as glutathione transferases, pose a challenge for detailed study by NMR spectroscopy. The human GST P1-1 observed in this study is a 46 kDa dimer. For these enzymes, a high level of protein deuteration is essential to acquire high-quality NMR spectra and to fulfill the requisite assignment problem. Deuteration has become a widely used technique for reducing nuclear spin relaxation in large biomolecules, resulting in increased signal intensity and resolution for multidimensional NMR experiments (*48, 49*). However, one problem associated with the expression of proteins from deuterated media is the necessity to back-exchange the deuterated amide sites for protons. If the protein of interest can be reversibly denatured, this is a trivial task. However, in the case of the GST dimers, slowly exchanging amide sites in the enzyme core cannot be readily exchanged in this manner while retaining a viable enzyme. Consequently, the number of detectable contiguous spin-systems is reduced by the presence of nonexchangeable amides. The presence of numerous gaps in the sequential connectivities exacerbates the assignment process by breaking linked spin-systems into short fragments that may be difficult to place within the primary sequence. We have previously reported near-complete chemical shift assignments for the 55 kDa human mu class enzyme, GST M2-2. In our study of GST M2-2, partially deuterated material was used to avoid the problems associated with slowly exchanging amide sites (*26*).

In the present study, our approach to the resonance assignment problem is targeted to the most solvent-exposed active site residues for GST P1-1. In this case, the NMR spectra are greatly simplified by only observing those amides that are readily exchangeable. Figure 1 shows that it was possible to assign the bulk of the exposed residues. In this instance, residue type identification by specific 1-^{13}C labeling provided essential information to correctly place the linked spin-system fragments in the primary sequence. In addition, local and long-range dipolar interactions obtained from 4D NOESY experiments are useful in bridging gaps in the sequential assignments.

Differences in the chemical shifts of the GSH complex versus the GS-hexyl complex identify several regions of the protein that are affected by the presence of the additional hexyl group (see Figure 6). These regions include all of α2 (residues 31−53) as well as some residues that flank α2. Additional chemical shift changes are also observed for Gln65, Ile69, Tyr109, Val200, and Asn205. Surprisingly, crystal structures of the GSH and GS-hexyl complexes show only a small number of structural differences due to the presence of the hexyl group. Specifically, residues 35−43 show a small displacement (0.5−1.6 Å, C_α) toward the bound hexyl group, and residues 207 and 208 show a 1 Å difference in their C_α positions. There are no other structural differences of significance between the two complexes. The chemical shift changes due to the presence of the hexyl group suggest the existence of additional structural changes beyond those that have been detected by X-ray crystallography. In particular, the environment of Tyr109, a residue implicated in catalysis of several hydrophobic substrates (*23*), is perturbed by the presence of the hexyl group. The effects on Tyr109 appear to be propagated to Asn205 which is directly below the side chain of Tyr109. Interestingly,

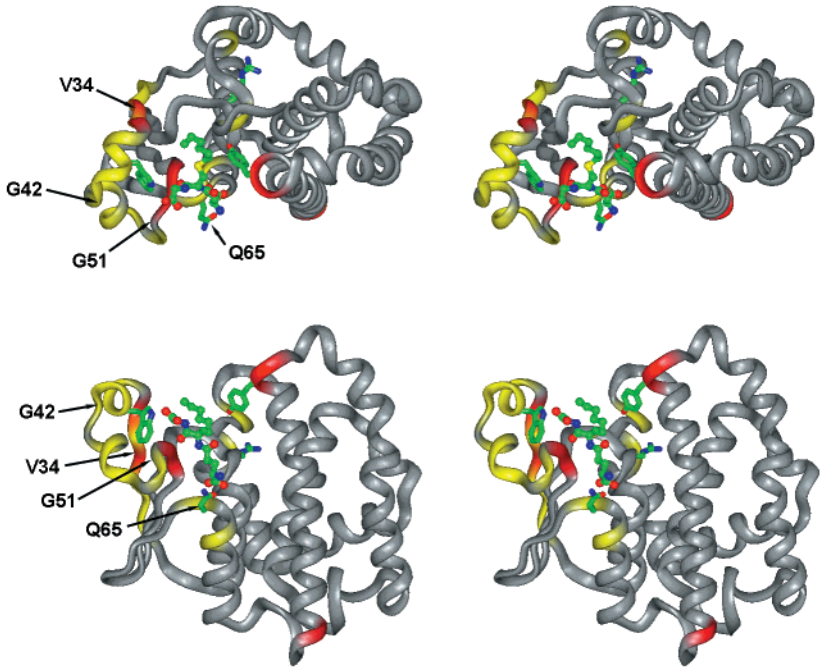

FIGURE 6: Chemical shift changes induced by the *S*-hexyl group. The locations of residues whose amide nitrogen and proton shifts differ between the GSH and GS-hexyl complex of GST P1-1 are mapped onto the structure of the GS-hexyl enzyme complex (1AQX, ref *18*). The upper part of the panel presents a relaxed stereoview of the enzyme from the top of the dimer, looking down the C_2 symmetry axis, into the active site. The lower part of the panel shows a stereoview looking from inside the enzyme toward the active site. Helix 2 is on the left-hand side of the protein in this view and colored red or yellow due to chemical shift changes between the GSH and GS-hexyl complex. Residues that show a chemical shift change [$\Delta\delta = (\delta_N^2 + \delta_H^2)^{1/2}$] of between 0.2 and 0.5 ppm are colored yellow. Residues that show a chemical shift change greater than 0.5 ppm are colored red. The largest chemical shift change was 1.25 ppm (residue 53). The remainder of the structure is colored gray to black. The bound glutathione is shown rendered in ball-and-stick and colored according to atom type. The side chains of Arg12, Trp39, Gln65, and Tyr109 are also shown, colored according to atom type. The locations of residues Val34, Gly42, Gly52, and Gln65 are indicated by the labeled arrows.

Val200, which is quite distant from the binding site, also shows a change in chemical shift due to the presence of the hexyl group. This effect appears to be mediated by changes in the position of the side chain of Arg12, a residue within the substate binding site. The actual size of the structural changes that are induced by the hexyl group awaits a detailed comparison of the structural differences between the GSH and GS-hexyl complexes in solution.

The initial attempt to assign the unliganded GST P1-1 was frustrated by the observation of fewer than expected amide resonance peaks in the NMR spectra. We were intrigued to find that the initial Monte Carlo assignment runs for the unliganded enzyme did not provide a reliable solution for residues in the solvent-exposed, active site α-helix, α2. Surprisingly, more resonance peaks appeared in the HMQC spectrum of GST P1-1 and some of the 2D HNCO spectra of the 1-^{13}C-labeled samples when the GS-hexyl ligand was bound. It became clear following the assignment of the GS-hexyl and GSH complexes, that the α2 resonance peaks were severely broadened due to chemical exchange in the unliganded enzyme at 306 K. These resonances, however, are clearly detectable in spectra of the unliganded enzyme acquired at lower temperatures.

The residues affected by temperature, Val34, Trp39, Gly42, and Gly51, are all found in the irregular alpha helix α2. This helix forms a significant part of the GSH binding site (see Figure 6). Consequently, it is not unexpected that these residues share common thermodynamic parameters (see Figure 4). The resonance line from Gln65 displays different behavior, broadening and disappearing at a significantly lower temperature. Gln65 is located between β4 and α3 and donates a main-chain hydrogen bond to Pro54 in the adjacent β-strand (β3). Since the hydrogen bond from Gln65 points back toward the active site and α3 is part of the dimer interface, the temperature dependence of the NMR resonance for this residue may reflect both changes in α2 as well cooperative interactions between monomers.

Thermodynamic Analysis of Local Unfolding. To account for the absence of resonance lines in the unliganded protein at high temperature, we propose that the region of the protein in the vicinity of α2 can exist in two conformational states in the unliganded enzyme. These two states undergo chemical exchange slowly on the time scale of the HMQC experiment because there is little change in the resonance line width for residues from this region of the protein as the temperature is raised. The first state, which is observed at low temperature, or in the presence of ligand, appears to be in a single conformation. The low-temperature structure of α2 in the unliganded enzyme appears to adopt a conformation similar to the GS-hexyl complex based upon the similarity in H_N, N, and C_α chemical shifts observed for the α2 residues. This conformation is similar to that observed in the crystal structure on the basis of NOE measurements. The second conformational state of GST P1-1, which is populated at higher temperatures in the absence of ligand, appears to consist of a manifold of different conformations that are in intermediate exchange on the time scale of the NMR experiment (milliseconds), such that the resonance lines are broadened beyond detection.

The enthalpy associated with this temperature-induced folding is on the order of −150 kJ/mol. This large enthalpy change clearly suggests that there is an extensive rearrange-

ment (folding) of α2 that occurs either at low temperatures or when ligand binds. Given the large size of this transition, it appears that the folding of both monomers is highly cooperative. This conclusion is supported by direct measurements of GSH binding to GST P1-1. Ricci and co-workers (*33*) have investigated the temperature dependence of GSH binding to GST P1-1 and have observed a large temperature dependence for the binding of the first GSH; the association constant decreases from 2.9×10^4 M^{-1} at 278 K to 0.077×10^4 M^{-1} at 316 K. In contrast, the second association constant shows a much smaller temperature dependence, decreasing from 5.5×10^3 M^{-1} at 278 K to 5.0×10^3 M^{-1} at 316 K. The small temperature dependence of the second association constant suggests that the binding of the first GSH changes the conformation of the second GSH binding site in a cooperative manner.

Information on the thermodynamics of the folding of α2 can be obtained from the temperature dependence of GSH binding. A van't Hoft plot (ln K_{eq} versus $1/T$) of the GSH binding data is highly curved, suggesting a large ΔC_p. Such large heat capacities are anticipated when binding is coupled to structural transitions (see *53*). If the folding of the α2 region is assumed to be highly cooperative, then the enthalpy associated with the folding can be obtained in a straightforward manner (*53*). If GSH has negligible affinity to GST P1-1 when α2 is unfolded, then the apparent binding enthalpy is given by eq 1:

$$\Delta H^\circ_{APP} = \Delta H^\circ_L - \Delta H^\circ_U K/(1 + K) \qquad (1)$$

where ΔH°_{APP} is the observed ΔH° for binding, ΔH°_L is the intrinsic enthalpy for ligand binding in the absence of the order−disorder transition, ΔH°_U is the enthalpy associated with unfolding of α2, and K is the equilibrium constant for the order-to-disorder transition.

The enthalphy of unfolding (ΔH°_U) can be obtained from the temperature dependence of GSH binding if we assume that the intrinsic enthalpy of binding of GSH to GST P1-1, ΔH°_L, is −20 kJ/mol. This value is based on direct measurement of the binding of GSH to GST M2-2, a class mu enzyme that does not undergo a ligand-induced disorder−order transition (*54*). Fitting the temperature-dependent binding data of Ricci and co-workers (*33*) to eq 1 gives a ΔH°_U of +120 kJ/mol (see Figure 7). This number is in good agreement with the value of ΔH°_U of +150 kJ/mol that was obtained from the analysis of the NMR data performed here.

In summary, the temperature (or ligand)-induced folding of α2 is a highly cooperative event; the folding of α2 in one monomer appears to induce the folding of α2 in the other monomer. The overall enthalpy associated with this transition is on the order of −120 to −150 kJ/mol. The enthalpy for folding of a helical segment the length of α2 is estimated to be −50 to −60 kJ/mol, based on model peptides (*50*−*52*). The difference between twice this sum and the observed ΔH° change likely reflects enthalpic gains due to side-chain interactions as well as due to rearrangement of core structural elements associated with the cooperative binding behavior.

The disorder−order transition of α2 explains a number of previous observations regarding the effect of temperature and mutations in α2 on GSH binding. As discussed above, the temperature dependence of GSH binding shows an apparent cooperativity that can be accounted for by the thermodynamics of folding of α2. It has also been shown that alteration of Gly42 and Gly51 to Ala markedly reduces the binding of GSH. Although it is possible that these changes have a direct effect on the interaction of the folded form of α2 with glutathione, as proposed by Lo Bello et al. (*32*), it is also possible that these mutations stabilize the unfolded states of α2 and thus affect GSH binding indirectly via the requisite structural transition of α2.

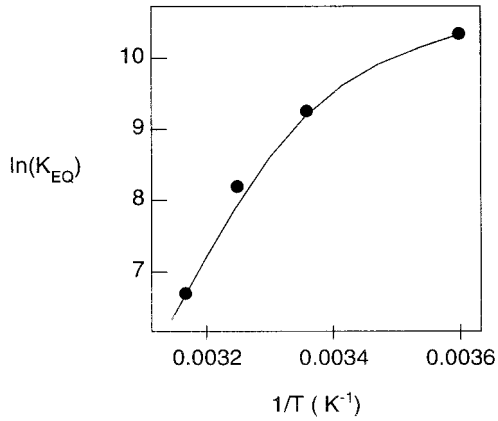

FIGURE 7: Temperature dependence of GSH binding. A van't Hoff plot of GSH binding is shown. The plotted points are the data presented by Caccuri et al. (*33*). The solid curve indicates the best fit to these data, giving a ΔH°_U of +120 kJ/mol for the folded-to-unfolded transition. This model assumes that the enthalpy associated with GSH binding to the completely folded enzyme is −20 kJ/mol (*54*).

Although the GSH-induced folding of α2 is a significant structural change toward the generation of a catalytically competent enzyme, the GSH−enzyme complex may not be an accurate description of the active form of the ternary complex. Chemical shift differences between the GSH and GS-hexyl form of the protein are suggestive of additional changes that occur due to the binding of the hydrophobic substrate. This hypothesis has also been proposed by Ricci and co-workers, who suggested that the binding of GSH is a multistep mechanism, with GSH binding first to a precomplex that then resolves to the catalytically active conformation (*55*). This scenario is also supported by transferred NOE experiments which suggest that the initial structure of the bound GSH is different than that observed in structural models derived from X-ray diffraction (*56*). Consequently, the formation of the functional active site may proceed in two steps. The first step corresponds to the temperature-induced folding of α2 observed in this work. The second step corresponds to additional rearrangements of the active site as the GSH−enzyme precomplex transitions to the active form of the enzyme.

CONCLUSION

We have clearly demonstrated that an extensive region of the class pi enzyme exists in multiple conformations in the unliganded form of the enzyme at physiological temperatures. The disorder-to-order transition associated with ligand binding is large on the basis of a thermodynamic analysis and would thus have a notable effect on the catalytic cycle of the enzyme. A significant portion of the free energy of GSH binding, −4 to −6 kJ/mol at 37 °C, is utilized to fold α2.

This free energy becomes available to markedly enhance product release after catalysis. The coupling between the structural transition of α2 and ligand binding has important consequences with respect to the rational design of inhibitors for this class of glutathione transferases. A significant amount of the free energy of the protein−ligand interaction is associated with a mechanistic step (folding of α2) that is indirectly related to the molecular details of protein−ligand interactions that are depicted in co-crystals of the complexes. The targeted design of inhibitors to GST P1-1 (*35*) needs to address the folding of α2 as part of the normal process of inhibitor binding. Finally, the disordered state of the unliganded enzyme may have significant implications in the regulation of GST P1-1 in normal and malignant tissues since the unfolded α2 is subject to inactivating trypsinolysis at Lys44 (*57*).

ACKNOWLEDGMENTS

We thank Dr. Gun Stenberg, Department of Biochemistry, Uppsala University, for kindly providing the pKXHP1 clone. We also thank V. Simplaceanu for his technical support of the NMR spectrometer.

REFERENCES

1. Armstrong, R. N. (1997) *Chem. Res. Toxicol. 10*, 2−18.
2. Eaton, D. L., and Bammler, T. K. (1999) *Toxicol. Sci. 49*, 156−164.
3. Ketterer, B. (1998) *Free Radical Res. Commun. 28*, 647−658.
4. Mannervik, B., Ålin, P., Guthenberg, C., Jensson, H., Tahir, M. K., Warholm, M., and Jörnvall, H. (1985) *Proc. Natl. Acad. Sci. U.S.A. 82*, 7202−7206.
5. Meyer, D. J., Coles, B., Pemple, S. E., Gilmore, K. S., Fraser, G. M., and Ketterer, B. (1991) *Biochem. J. 274*, 409−414.
6. Meyer, D. J., and Thomas, M. (1995) *Biochem. J. 311*, 739−742.
7. Pemble, S. E., Wardle, A. F., and Taylor, J. B. (1996) *Biochem. J. 319*, 749−754.
8. Board, P. G., Baker, R. T., Chelvanayagam, G., and Jermiin, L. S. (1997) *Biochem. J. 328*, 929−935.
9. Board, P. G., Coggan, M., Chelvanayagam, G., Easteal, S., Jermiin, L. S., Schulte, G. K., Danley, D. E., Hoth, L. R., Griffor, M. C., Kamath, A. V., Rosner, M. H., Chrunyk, B. A., Perregaux, D. E., Gabel, C. A., Geoghegan, K. F., and Pandit, J. (2000) *J. Biol. Chem. 275*, 24798−24806.
10. Bruns, C. M., Hubatsch, I., Ridderström, M., Mannervik B., and Tainer, J. A. (1999) *J. Mol. Biol. 288*, 427−439.
11. Cameron, A. D., Sinning, I., L'Hermite G., Olin, B., Board, P. G., Mannervik, B., and Jones, T. A. (1995) *Structure 15*, 717−727.
12. Sinning, I., Kleywegt, G. J., Cowan, S. W., Reinemer, P., Dirr, H. W., Huber, R., Gilliland, G. L., Armstrong, R. N., Ji, X., Board, P. G., Olin, B., Mannervik, B., and Jones, T. A. (1993) *J. Mol. Biol. 232*, 192−212.
13. Patskovska, L. N., Fedorov, A. A., Patskovsky, Y. V., Almo, S. C., and Listowsky, I. (1998) *Acta Crystallogr., Sect. D: Biol. Crystallogr. 54*, 458−460.
14. Raghunathan, S., Chandross, R. J., Kretsinger, R. H., Allison, T. J., Penington, C. J., and Rule, G. S. (1994) *J. Mol. Biol. 238*, 815−832.
15. Ji, X., Zhang, P., Armstrong, R. N., and Gilliland, G. L. (1992) *Biochemistry 31*, 10169−10184.
16. Ji, X., Armstrong, R. N., and Gilliland, G. L. (1993) *Biochemistry 32*, 12949−12954.
17. Oakley, A. J., Lo Bello, M., Ricci, G., Federici, G., and Parker, M. W. (1998) *Biochemistry 37*, 9912−9917.
18. Prade, L., Huber, R., Manoharan, T. H., Fahl, W. E., and Reuter, W. (1997) *Structure 5*, 1287−1295.
19. Reinemer, P., Dirr, H. W., Ladenstein, R., Huber, R., Lo Bello, M., Federici, G., and Parker, M. W. (1992) *J. Mol. Biol. 227*, 214−226.
20. Rossjohn, J., McKinstry, W. J., Oakley, A. J., Verger, D., Flanagan, J., Chelvanayagam, G., Tan, K. L., Board, P. G., and Parker, M. W. (1998) *Structure 6*, 309−322.
21. Dirr, H., Reinemer, P., and Huber, R. (1994) *Eur. J. Biochem. 220*, 645−661.
22. Widersten, M., Kolm, R. H., Björnestedt, R., and Mannervik, B. (1992) *Biochem. J. 285*, 377−381.
23. Lo Bello, M., Oakley, A. J., Battistoni, A., Mazzetti, A. P., Muccetelli, M., Mazzarese, G., Rossjohn, J., Parker, M. W., and Ricci, G. (1997) *Biochemistry 36*, 6207−6217.
24. McCallum, S. A., Hitchens, T. K., and Rule G. S. (2000) *Biochemistry 39*, 7343−7356.
25. Jemth, P., and Mannervik, B. (2000) *J. Biol. Chem. 275*, 8618−8624.
26. McCallum, S. A., Hitchens, T. K., and Rule, G. S. (1999) *J. Mol. Biol. 285*, 2119−2132.
27. Stella L., Caccuri, A. M., Rosato, N., Nicotra, M., Lo Bello, M., De Matteis, F., Mazzeti, A. P., Federici, G., and Ricci, G. (1998) *J. Biol. Chem. 273*, 23267−23273.
28. Ricci, G., Caccuri, A. M., Lo Bello, M., Rosato, N., Mei, G., Nicotra, M., Chiessi, E., Mazzetti, A. P., and Federici, G. (1996) *J. Biol. Chem. 271*, 16187−16192.
29. Ricci, G., Del Boccio, G., Pennelli, A., Lo Bello, M., Petruzelli, R., Caccuri, A. M., Barra, D., and Federici, G. (1991) *J. Biol. Chem. 266*, 21409−21415.
30. Stella, L., Nicotra, M., Ricci, G., Rosato, N., and Di Iorio, E. E. (1999) *Proteins: Struct., Funct., Genet. 37*, 1−9.
31. Stella, L., Di Iorio, E. E., Nicotra, M., and Ricci, G. (1999) *Proteins: Struct., Funct., Genet. 37*, 10−19.
32. Lo Bello, M., Nuccetelli, M., Chiessi, E., Lahm, A., Mazzetti, A. P., Battistoni, A., Caccuri, A. M., Oakley, A. J., Parker, M. W., Tramontano, A., Federici, G., and Ricci, G. (1998) *J. Mol. Biol. 284*, 1717−1725.
33. Caccuri, A. M., Antonini, G., Ascenzi, P., Nicotra, M., Nuccetelli, M., Mazzetti, A. P., Federici, G., Lo Bello, M., and Ricci, G. (1999) *J. Biol. Chem. 274*, 19276−19280.
34. Wright, P. E., and Dyson, H. J. (1999*) J. Mol. Biol. 293*, 321−331.
35. Satyam, A., Hocker, M. D., Kane-Maguire, K. A., Morgan, A. S., Villar, H. O., and Lyttle, M. H. (1996) *J. Med. Chem. 39*, 1736−1747.
36. Batist, G., Tuluple, A., Sinha, B. K., Katki, A. G., Myers, C. E., and Cowan, K. H. (1986) *J. Biol. Chem. 261*, 15544−15549.
37. Mannervik, B., Castro, V. M., Danielson, U. H., Tahir, M. K., Hansson, J., and Ringborg, U. (1987) *Carcinogenesis 8*, 1929−1932.
38. Moscow, J. A., Townsend, A. J., Goldsmith, M. E., Whang-Peng, J., Vickers, P. J., Poisson, R., Legault-Poisson, S., Myers, C. E., and Cowan, K. H. (1988) *Proc. Natl. Acad. Sci. U.S.A. 85*, 6518−6522.
39. Puchalski, R., and Fahl, W. E. (1990) *Proc. Natl. Acad. Sci. U.S.A. 87*, 2443−2447.
40. Tsuchida, S., and Sato, K. (1992) *Crit. Rev. Biochem. Mol. Biol. 27*, 337−384.
41. Caffery P. B., Zhu, M., Zhang, Y., Chinen N., and Frenkel, G. D. (1999) *Cancer Lett. 136*, 47−52.
42. Kolm, R. H., Stenberg, G., Widersten, M., and Mannervik, B. (1995) *Protein Expression Purif. 6*, 265−271.
43. Habig, W. H., and Jakoby, W. B. (1981) *Methods Enzymol. 77*, 398−405.
44. Marion, D., Ikura, M., and Bax, A. (1989) *J. Magn. Reson. 84*, 425−430.
45. Bax, A., and Pochapsky, S. S. (1992) *J. Magn. Reson. 99*, 638−643.
46. Skelenar, V., Piotto, M., Leppik, R., and Saudek, V. (1993) *J. Magn. Reson. 102*, 241−245.
47. Gruschus, J. M., and Ferretti, J. A. (1998) *J. Magn. Reson. 135*, 87−92.
48. Sattler, M., and Fesik, S. W. (1996) *Structure 4*, 1245−1249.

49. Goto, N. K., and Kay, L. E. (2000) *Curr. Opin. Struct. Biol. 10*, 585−592.
50. Scholtz, J. M., Marquesee, S., Baldwin, R. L., York, E. J., Stewart, J. M., Santoro, M., and Bolen, D. W. (1991) *Proc. Natl. Acad. Sci. U.S.A. 88*, 2854−2858.
51. Rialdi, G., and Hermans, J. (1966) *J. Am. Chem. Soc. 88*, 5719−5720.
52. Chou, P. Y., and Scheraga H. A. (1971) *Biopolymers 10*, 675−680.
53. Eftink, M. R., Anusieum, A. C., and Biltonen, R. L. (1983) *Biochemistry 22*, 3884−3896.
54. Penington, C. (1994) Ph.D. Dissertation, University of Virginia.
55. Caccuri, A. M., Lo Bello, M., Nuccetelli, M., Nicotra, M., Rossi, P., Antonini, G., Federici, G., and Ricci, G. (1998) *Biochemistry 37*, 3028−3034.
56. Nicotra, M., Paci, M., Sette, M., Oakley, A. J., Parker, M. W., Lo Bello, M., Caccuri, A. M., Federici, G., and Ricci, G. (1998) *Biochemistry 37*, 3020−3027.
57. Lo Bello, M., Pastore, A., Petruzelli, R., Parker, M. W., Wilce, M. C. J., Federici, G., and Ricci, G. (1993) *Biochem. Biophys. Res. Commun. 194*, 804−811.
58. Connolly, M. L. (1993) *Science 221*, 709−713.

BI010909+